ISSN (Print) 1226-1750
ISSN (Online) 2233-6656
Journal of Magnetics 24(4), 791-798 (2019) https://doi.org/10.4283/JMAG.2019.24.4.791

Equivalent Magnetic Circuit Model for Consequent Pole Hybrid Excitation Synchronous Machine with AC Field Control

Jie Wu[1]*, Jing Yin[1], Baixing Zhuang[2], Mingjie Wang[1], and Jitao Zhang[1]

[1]Dept. Electrical Engineering, Zhengzhou University of Light Industry, Henan 450002, China
[2]ANSYS, Shenzhen, Guangdong 518048, China

(Received 15 July 2018, Received in final form 3 October 2019, Accepted 7 October 2019)

At present, almost all hybrid excitation machines (HEMs) apply DC field current to control the air-gap flux. However, the DC field control mode results in a problem that the capability of field-weakening is not equal to that of field-strengthening. This paper briefly explains the mechanism of asymmetric bidirectional field control capability in present HEMs, proposes a consequent pole hybrid excitation synchronous (CPHES) machine with AC field control mode to solve the asymmetric problem. The structure and principles of CPHES machine are presented. Additionally, the equivalent magnetic circuit model of CPHES machine is derived to reduce the computational complexity of analyzing CPHES structure by using three-dimensional finite element analysis (3D-FEA). The proposed equivalent model and 3D-FEA are compared, the results verify the proposed model is basically consistent with the 3D-FEA, and the proposed model is able to reduce the computational complexity greatly.

Keywords : AC field control, consequent pole, equivalent magnetic circuit, hybrid excitation machine

1. Introduction

Compared to the electrical excitation machines, the permanent magnet (PM) machines generate a magnetic field through PM poles, eliminating the excitation device and improving the efficiency of the machine. However, it is difficult to regulate the air-gap magnetic field of PM machines, which is one of the key factors that restrict the development of PM machines. Hybrid excitation machines (HEMs) can solve this problem. It is assembled with both PMs and electric excitation windings. The two magneto-motive forces (MMFs) work together to generate the main field of the machine, which is able to realize the adjustment and control of the air-gap magnetic field of the machine, thereby improving its performance.

Most of the existing HEMs use direct current to adjust the air-gap field, such as consequent pole permanent magnet (CPPM) machines [1], hybrid excited claw-pole machines [2], hybrid excited flux switching machines [3, 4], parallel hybrid excitation machines [5], hybrid excitation doubly salient machines [6, 7], HEMs with isolated magnetic paths [8], hybrid excited flux reversal machines [9, 10], HEMs with field adjustment at end-side [11], etc. The HEMs with DC field control mode has its advantages. First of all, the magnetic structure is easy to understand, the magnetic path coupling DC field windings and the armature or PM poles can explain the principles of field adjustment. Additionally, the inductance of DC field winding is small, the bidirectional field control capability is obtained by adjusting the amplitude and direction of the DC excitation current, so it is easy to implement the field control.

However, there is an inevitable problem with the HEMs employing DC excitation. There are three different MMFs in HEMs, which are generated by DC field windings, AC armature windings and PM poles, noted as F_f, F_a, and F_{pm}, respectively. Taking the CPPM machine as an example, the magnetic field always goes through the path with the smallest reluctance, so the phase of F_f is always fixed on d-axis, then its phase thereof cannot be adjusted. In the field-weakening, the F_f is always opposite to F_{pm}, while in field-strengthening, the F_f is always in phase with F_{pm}, as shown in Fig. 1. Noting the resultant MMF of F_{pm} and F_a as F_0, it can be proved that

*Corresponding author: Tel: +86-13733170917
Fax: +86-371-63556790, e-mail: defermat2008@hotmail.com

This paper was presented at the IcAUMS2018, Jeju, Korea, June 3-7, 2018.

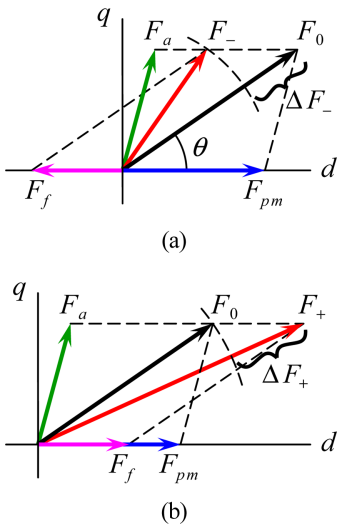

Fig. 1. (Color online) (a) filed-weakening. (b) field-strengthening.

$$\left|F_0\right|-\left|F_-\right|\le\left|F_+\right|-\left|F_0\right| \tag{1}$$

which means in the HEMs with DC excitation the bidirectional field control capability is asymmetric. In general, the demagnetization effect is inferior to the magnetization effect.

While the field-weakening capability could be extended by adjusting the DC field current for the HEMs employing DC excitation, and then the similar range of demagnetization and magnetization could be obtained. However, there is no doubt that the field current levels are not equal in either case. If the same regulating range is to be obtained, the field weakening current is higher than the field strengthening current. Therefore, the feed-back control method in the HEMs with DC-mode can not provide symmetric bidirectional flux control capability.

In practice, symmetric bidirectional field control capability is of significance to HEMs. In general, it is more difficult to achieve field-weakening than field-strengthening in PM machines, which means field-weakening requires higher field current at the same level of field control. Excessive field-weakening current may permanently demagnetize the PM poles, and then it is a huge risk for PM machines. Moreover, higher field current results in higher excitation loss. Additionally, the maximum speed of the motor depends on the field-weakening capability, and the volumetric power density of the motor is related to the maximum speed. In summary, the symmetric bidirectional flux control capability helps to extend the speed range, to improve the volumetric power density of the motor, to decrease the risk of demagnetization, and to reduce the excitation loss at demagnetization.

In order to solve the asymmetric problem mentioned above, the field control with AC excitation is crucial to HEMs [12]. This paper focuses on the HEM with consequent pole rotor and AC field control windings. By adjusting the magnitude and phase of the current flowing into the 3-phase AC field winding, the F_f and F_0 can always be in a line, then the demagnetization and magnetization are symmetrical.

In this paper, the principles of consequent pole hybrid excitation synchronous (CPHES) machine are introduced firstly. Because there are three rotating magnetic fields in CPHES machine, and they couple each other in three orthogonal directions, it is difficult to present the equivalent magnetic circuit in a single circuit. According to the two-reaction theory, this paper proposes to decompose the equivalent magnetic circuit of CPHES machine into d- and q-axis equivalent magnetic circuit, and then synthesize the obtained d- and q-axis armature reaction fluxes to obtain the resultant flux linkage coupling with one phase winding, finally obtain the back-EMF. The results are compared with the 3D finite element analysis (3D-FEA) to verify the proposed equivalent magnetic circuit model.

2. Structure and Principles

The structure of CPHES machine is shown in Fig. 2. The rotor structure of this machine is basically the same as the CPPM rotor. There are two sets of 3-phase AC windings on its stator, i.e. armature windings and field windings, which are staggered in the circumferential and in the axial direction, as shown in Fig. 3. Apparently, the phase of F_f can be adjusted flexibly by controlling the field current.

When the machine is loaded, the time phase of field current is adjusted so that F_f is in phase with F_0 in space, then the resultant air-gap MMF is $F_0 + F_f$, and the air-gap magnetic field is strengthened; if the time phase of field

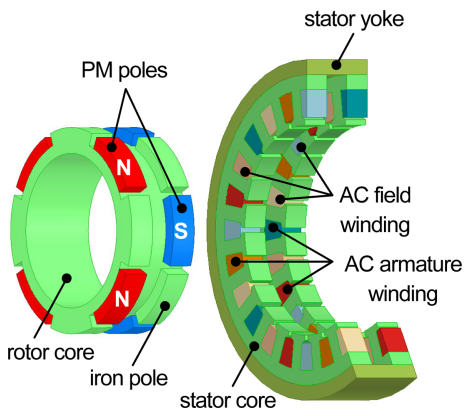

Fig. 2. (Color online) Topology of the CPHES machine.

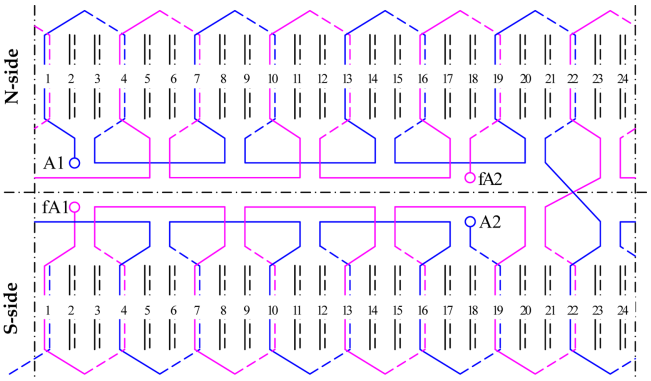

Fig. 3. (Color online) Winding connection of phase-A.

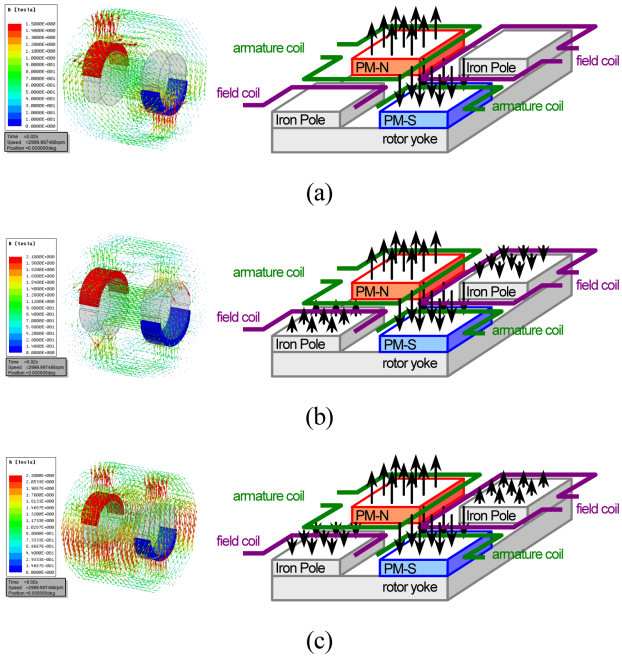

Fig. 4. (Color online) The air-gap field distribution and flux path under three different conditions of AC field current. (a) no field current; (b) field weakening; and (c) field strengthening.

current is adjusted so that F_f is out of phase with F_0 in space, then the resultant air-gap MMF is $F_0 - F_f$, and the air-gap magnetic field is weakened. Therefore in CPHES machine, the demagnetization equals to magnetization.

Fig. 4 shows that, in the field-strengthening, the iron pole at N-side is induced as S-pole, and the iron pole at S-side is induced as N-pole. The field-weakening is a different situation, the iron pole at N-side is induced as N-pole, and the iron pole at S-side is induced as S-pole.

3. Equivalent Magnetic Circuit

According to the structure and principles of the CPHES machine, there are three rotating magnetic fields in the structure, namely PM field, armature field and excitation field, and the three magnetic fields are simultaneously coupled in the radial, tangential and axial directions. The CPHES machine is, therefore, a multi-directional coupling system consisting of multiple excitation sources and multiple rotating magnetic fields. In this section, an equivalent magnetic circuit model of CPHES machine is established based on the 3D-FEA.

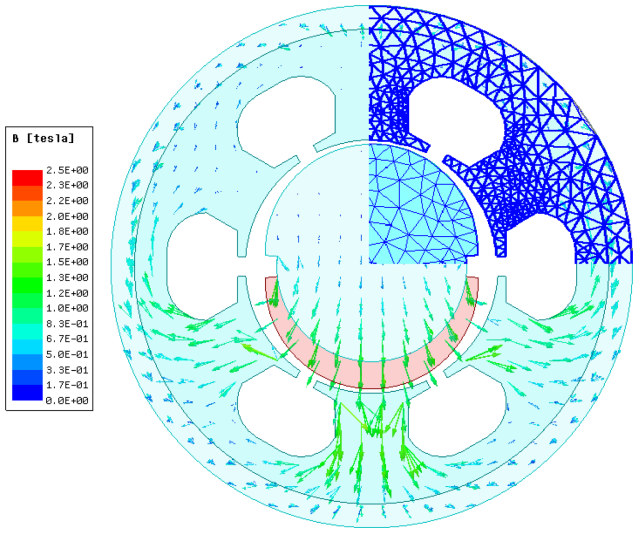

Fig. 5. (Color online) Mesh grid and flux path at N-side due to magnets only. There is few flux goes through the air-gap over iron pole at N-side under the condition of zero field current.

Since the resultant magnetic field is determined by the amplitude and spatial position of the three magnetic field components, if the three components are respectively projected on the d-axis and the q-axis, then the d- and q-axis equivalent magnetic circuits could be obtained. Subsequently, the equivalent magnetic field of each axis can be derived by their equivalent magnetic circuits, respectively. The two-reaction theory has revealed that the flux linked with one phase winding can be solved by combining d- and q-axis magnetic field. Therefore, the d- and q-axis equivalent magnetic circuit could be used to solve the resultant air-gap field of CPHES machine.

Fig. 5 depicts the field distribution at N-side in detail due to magnets only. Fig. 5 shows that, when the PM poles act only, the magnetic flux passes from the PM N-pole to the PM S-pole through the axial magnetic path. There is few flux goes through the air-gap over iron pole under the condition of zero field current.

Fig. 6 displays the field distribution at N-side due to electric excited field only at two typical rotor positions. It can be found that, whether the electric excited MMF acts on the d-axis or the q-axis, the magnetic flux on both

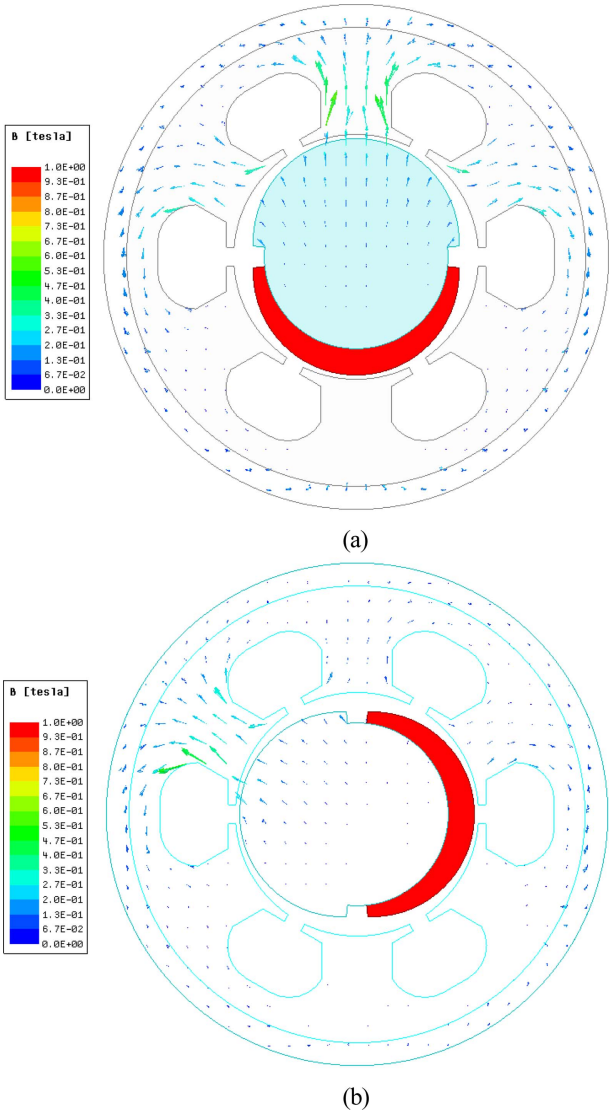

Fig. 6. (Color online) Flux path at N-side as only electric excited field acts on (a) d-axis over iron pole and on (b) q-axis.

sides is connected by the axial magnetic field. When the electric excited MMF acts on the q-axis, the flux mainly goes through the air-gap over half of the iron pole, the rest flux passes through the air-gap over half of the PM pole.

According to the above analysis, if the saturation is not considered, the d- and the q-axis equivalent magnetic circuits of the CPHES machine are shown in Fig. 7 and Fig. 8, respectively.

4. Analysis of Reluctance

The equivalent magnetic circuit contains multiple different magnetic reluctances. The following calculates the magnetic reluctance of each part. Fig. 9 shows the cross-section of CPHES machine.

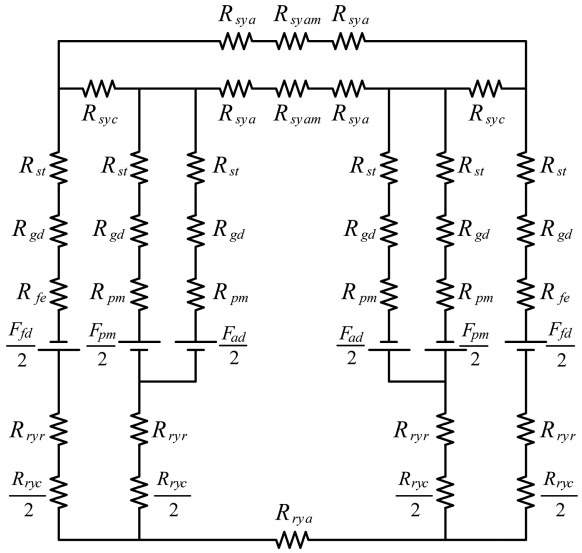

Fig. 7. The equivalent magnetic circuit of the d-axis.

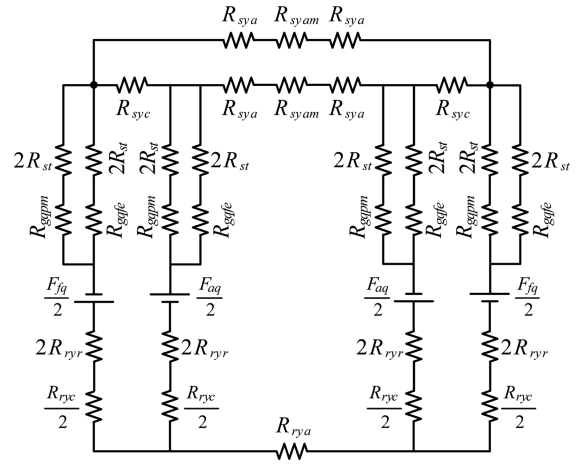

Fig. 8. The equivalent magnetic circuit of the q-axis.

4.1. PM Poles

The axial length of the PM pole is L, then the reluctance of PM pole is

$$R_{pm} = \frac{h_{pm}}{\mu_0 A_{pm}} \tag{2}$$

where μ_0 is the vacuum permeability, and A_{pm} the average area of PM pole. Let α_{pm} be the PM pole arc coefficient, and p the number of pole pairs, then

$$A_{pm} = \frac{\alpha_{pm}\pi L}{p}\left(r_{or} + \frac{1}{2}h_{pm}\right) \tag{3}$$

4.2. Iron Poles

The axial length of iron pole is L, then the reluctance of

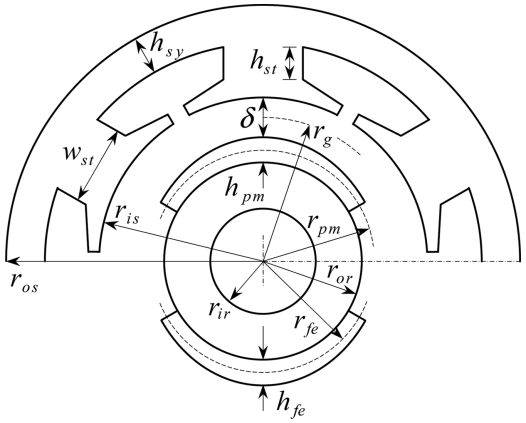

Fig. 9. Cross-section of CPHES machine.

iron pole is

$$R_{fe} = \frac{k_{fe} h_{fe}}{\mu_0 \mu_{fe} A_{fe}} \tag{4}$$

$$A_{fe} = \frac{\alpha_{fe} \pi L}{p}(r_{or} + \frac{1}{2} k_{fe} h_{fe}) \tag{5}$$

where μ_{fe} is the permeability of ferromagnetic material, and A_{fe} the average area of iron pole, α_{fe} the pole arc coefficient of iron pole, k_{fe} the coefficient of equivalent thickness.

4.3. Air-gap

The air-gap reluctance is crucial to the equivalent magnetic circuit. Due to the d- and q-axis decomposition, the air-gap reluctance should be divided into two parts, i.e. the d- and the q-axis air-gap reluctance. The d-axis air-gap reluctance is noted as R_{gd}. The q-axis air-gap reluctances over PM-pole and iron pole are noted as R_{gqpm} and R_{gqfe}, respectively.

$$R_{gd} = \frac{\delta}{\mu_0 A_{gd}} \tag{6}$$

$$A_{gd} = \frac{\alpha_{pm} \pi r_g L}{p} \tag{7}$$

$$R_{gqpm} = \frac{2(\delta + h_{pm})}{\mu_0 A_{pm}} \tag{8}$$

$$R_{gqfe} = \frac{2\delta}{\mu_0 A_{fe}} + \frac{2h_{fe}}{\mu_0 \mu_{fe} A_{fe}} \tag{9}$$

4.4. Stator Core

The flux paths are various in different field control states. The reluctance in stator core includes stator tooth reluctance R_{st}, circumferential reluctance of stator yoke R_{syc}, axial reluctance of side stator yoke R_{sya} and middle stator yoke R_{syam}.

$$R_{st} = \frac{2ph_{st}}{\mu_0 \mu_{si} w_{st} L N_s}, \tag{10}$$

$$R_{syc} = \frac{\pi r_{sy}}{3p\mu_0 \mu_{si} h_{sy} L}, \tag{11}$$

$$R_{sya} = \frac{0.5pL}{\mu_0 \mu_{si} \pi r_{sy} h_{sy}}, \tag{12}$$

$$R_{syam} = \frac{pL_{syam}}{2\mu_0 \mu_{si} \pi r_{sym} h_{sym}}, \tag{13}$$

where μ_{si} is the relative permeability of stator core, L the axial length of stator core at N-side or S-side, N_s the number of slots, L_{syam} the magnetic path length of middle stator yoke in the axial direction, r_{sym} and h_{sym} the radius and the thickness of middle stator yoke, r_{sy} the average radius of stator yoke,

$$r_{sy} = r_{os} - \frac{1}{2} h_{sy}. \tag{14}$$

4.5. Rotor Yoke Core

The inductance of rotor yoke includes radial, circumferential and axial components, noted as R_{ryr}, R_{ryc} and R_{rya}, respectively. Let L_{rya} be the average magnetic path length of rotor yoke in axial direction, then

$$R_{ryr} = \frac{p(r_{or} - r_{ir})}{\mu_0 \mu_{fe} \pi (r_{or} + r_{ir}) L} \tag{15}$$

$$R_{ryc} = \frac{\pi (r_{or} + r_{ir})}{2\mu_0 \mu_{fe} p (r_{or} - r_{ir}) L} \tag{16}$$

$$R_{rya} = \frac{L_{rya}}{\mu_0 \mu_{fe} \pi (r_{or}^2 - r_{ir}^2)} \tag{17}$$

Table 1 lists the main dimensions of a 24-slot/8-pole

Table 1. Main Dimensions of a CPHES Model.

Model	Value	Model	Value	Model	Value
r_{os}	65 mm	w_{st}	4.8 mm	r_{or}	30 mm
r_{is}	34.5 mm	δ	1.3 mm	r_{ir}	15 mm
h_{sy}	10 mm	L	85 mm	h_{pm}	3.2 mm

Table 2. Part Reluctances of the Model in Table 1.

Reluctance	Value/H^{-1}	Reluctance	Value/H^{-1}
R_{pm}	1.44×10^6	R_{fe}	718
R_{gd}	5.45×10^5	R_{ryr}	5960
R_{gq}	1.04×10^5	R_{ryc}	1838
R_{st}	3346	R_{sya}	3.06×10^4
R_{syc}	5515	R_{rya}	1.63×10^5

CPHES model. The reluctances are shown in Table 2.

5. Verification

In order to verify the proposed equivalent magnetic circuit model, the 3D-FEA results are compared with the results of equivalent magnetic circuit. Taking the back-EMF of one phase armature winding as an example, the two methods are compared under the conditions of no-load and loading with field control.

When using the equivalent magnetic circuit method, there are two problems that need to be clarified first. One is the magnitude of the F_{pm}, and the other is the angle between F_0 and F_{pm}. This section first gives the determination method of these two parameters, and then compares the calculation results.

5.1. Determination of F_{pm} and Angle θ

According to the operating principle of the CPHES machine, the position of F_f in loading field control should be determined according to the position of F_0. In fact, the position of F_0 in space is also the angle θ between F_0 and F_{pm} as shown in Fig. 1(a). Obviously, the angle θ is determined by F_{pm} and F_a.

According to the AC winding theory, the magnitude of F_a can be directly determined by the armature current. If F_a is fixed on the q-axis, the following formula holds,

$$F_{pm} = \frac{F_a}{\tan\theta}. \tag{18}$$

Then the problem turns into how to determine the angle θ.

The angle θ is the offset of the loading air-gap field relative to the no-load air-gap field, which will vary the time phase of back-EMF in armature winding. The time phase of the back-EMF strictly corresponds to the spatial position of the MMF, so the angle θ can be determined through the phase shift of back-EMF.

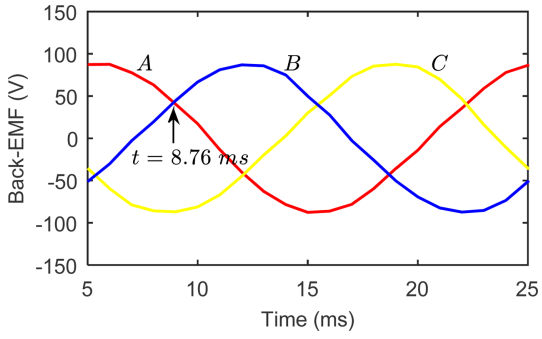

Fig. 10. (Color online) The no-load back-EMFs in armature winding.

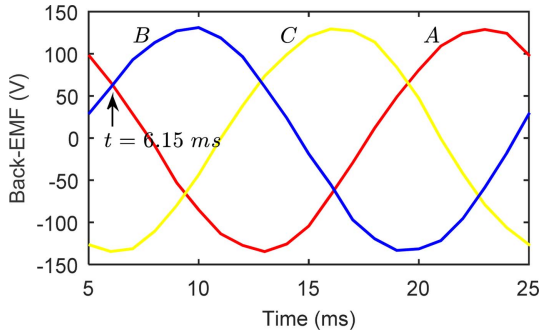

Fig. 11. (Color online) The loading back-EMFs in armature winding.

Fig. 10 and Fig. 11 show the back-EMF waveforms of 3-phase armature winding with no-load and armature current of 5A, respectively, where the F_a is on the q-axis.

It can be seen from the figures that, the back-EMF of phase A intersects with phase B at 8.76 ms under no-load condition without field control, and they intersect with each other at 6.15 ms under loading condition without field control. It means the back-EMF of armature winding is shifted by 2.61 ms, i.e. $\theta = 46.9°$ electrical angle, then

$$F_{pm} = \frac{F_a}{\tan 46.9°} = 808.26\,\text{A} \tag{19}$$

5.2. No-load with Field Control

Under the no-load condition with field control, the resultant air-gap field is formed by F_{pm} and F_f, both of them are on d-axis, then the d- and q-axis components of F_f are

$$F_{fd} = F_f \tag{20}$$

$$F_{fq} = 0 \tag{21}$$

If the field current is 1A with field-strengthening, the d-axis component of F_f is

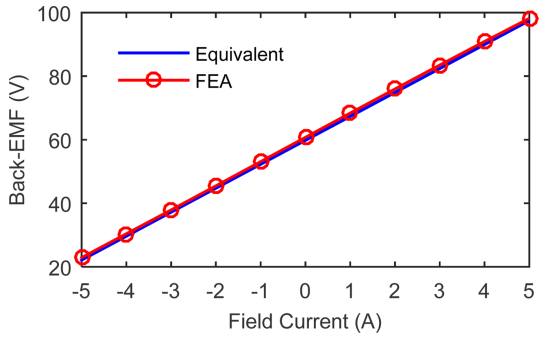

Fig. 12. (Color online) Comparison of no-load back-EMF by equivalent magnetic circuit and 3D-FEA when the field current varies from 5A in field-weakening to 5A in field-strengthening.

$$F_{fd} = 1.35\frac{N_f k_{wf}}{p} I_f = 86.4\text{A}. \quad (22)$$

Substituting Eq. (22) into the equivalent magnetic circuit model, the flux linking with one-phase armature winding can be obtained,

$$\Phi_a = 5.94\times10^{-4}\ \text{Wb}, \quad (23)$$

so the back-EMF of one-phase armature winding is

$$E_a = 4.44 f N_a \Phi_a k_{wa} = 67.6\text{V}. \quad (24)$$

According to the above method, the back-EMF of one-phase armature winding under no-load condition with different field current can be obtained.

Fig. 12 shows the variation of the no-load back-EMF of one-phase armature winding when the field current varies between field strengthening 5A and field weakening 5A. It can be found that the armature back-EMF increases linearly with the field current, which means under no-load condition the CPHES machine has bidirectional symmetric field control capability. Additionally, the results of the equivalent magnetic circuit are basically consistent with 3D-FEA.

5.3. Loading with Field Control

Under the loading condition with field control, the resultant air-gap field is formed by F_{pm}, F_a and F_f. Given the armature current I_a is 5A, and the F_a is fixed on the q-axis, then the d- and q-axis components of F_a are

$$F_{ad} = 0 \quad (25)$$

$$F_{aq} = F_a \quad (26)$$

According to the foregoing analysis, the angle between F_f and the d-axis is 46.9°.

It should be noted that, for convenience of illustration, the current is fixed on the q-axis in the example. In fact, the magnitude of the armature current can be other values, and the phase is not limited to the q-axis and can be at any position.

If the field current is 5A with field-weakening, the MMFs are calculated as follows,

$$F_a = 1.35\frac{N_a k_{wa}}{p} I_a = 864\text{A} \quad (27)$$

$$F_f = 1.35\frac{N_f k_{wf}}{p} I_f = 432\text{A} \quad (28)$$

$$F_{fd} = F_f \cos\theta = 295.17\text{A} \quad (29)$$

$$F_{fq} = F_f \sin\theta = 315.43\text{A} \quad (30)$$

By substituting the above values into the equivalent magnetic circuit, the flux linking with one-phase armature winding can be obtained,

$$\Phi_a = \sqrt{\Phi_{ad}^2 + \Phi_{aq}^2} = 3.53\times10^{-4}\ \text{Wb}, \quad (31)$$

so the back-EMF of one-phase armature winding is

$$E_a = 4.44 f N_a \Phi_a k_{wa} = 40.09\text{V}. \quad (32)$$

According to the above method, the back-EMF of one-phase armature winding under different field currents with 5A armature current can be obtained.

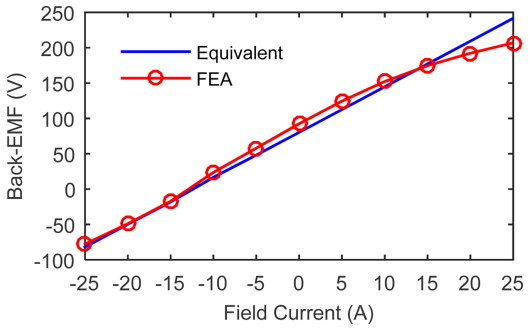

Fig. 13. (Color online) Comparison of loading back-EMF by equivalent magnetic circuit and 3D-FEA when the field current varies from 25A in field-weakening to 25A in field-strengthening.

Fig. 13 shows the variation of back-EMF fundamental in one-phase armature winding when the field current varies between field strengthening 25A and field weakening 25A. It can be found that, when the field-strengthening current is applied, the air-gap field increases as the field current is rising, so does the back-EMF. In field-weakening, the air-gap field gradually decreases with the increase of the field current, and the back-EMF gradually drops also. As the field-weakening current increases to a certain extent, the air-gap field is feeble. The air-gap field will be reversed if the field-weakening current continues to increase, and the back-EMF amplitude will gradually rise again. The phase of back-EMF is not displayed in Fig. 13, but the negative value of the back-EMF fundamental amplitude indirectly reflects the reverse of phase. It should be noted that it is meaningless to weaken the air gap field to zero.

In the equivalent magnetic circuit model, the influence of magnetic circuit saturation is ignored. Therefore, the back-EMF in the equivalent magnetic circuit method varies linearly with the field current. However, the finite element method considers the saturation. When the excitation current is large, especially in the field-strengthening region, the back-EMF varies nonlinearly with the excitation current, which causes difference in Fig. 13.

Based on the above calculation results, it can be found

that the proposed equivalent magnetic circuit model is basically consistent with the FEA results under both no-load and loading condition, which indicates that it is feasible to analyze the CPHES machine by the proposed equivalent magnetic circuit model.

6. Conclusions

The CPHES machine is a new type of hybrid excitation synchronous machine, its electromagnetic structure is complex, and 3D-FEA requires a long computing time. This paper proposed the d-axis and q-axis equivalent magnetic circuit model of CPHES machine. The proposed method is compared with 3D-FEA, the results of the two methods are consistent, so it is feasible to analyze the CPHES machine by the proposed equivalent magnetic circuit model. In the computing, the proposed equivalent magnetic circuit model spent about 1 minute, but 3D-FEA took about 10 days. Therefore, the proposed method has significant advantages in computational complexity, which will lay the foundation for further study of the CPHES machine.

Acknowledgment

This work was supported in part by the Natural Science Foundation of Henan Province under Grant 162300410319, and the office of Science and Technology in Henan Province under Grant 172102310254.

References

[1] J.-A. Tapia, F. Leonardi, and T.-A. Lipo, IEEE Trans. Ind. Appl. **39**, 6 (2003).
[2] R. Rebhi, A. Ibala, and A. Masmoudi, IEEE Trans. Ind. Appl. **51**, 1 (2015).
[3] W. Hua, G. Zhang, and M. Cheng, IEEE Trans. Ind. Electron. **62**, 9 (2015).
[4] G. Zhang, W. Hua, M. Cheng, and J.-G. Liao, IEEE Trans. Ind. Appl. **51**, 5 (2015).
[5] W.-W. Geng, Z.-R. Zhang, K. Jiang, and Y.-G. Yan, IEEE Trans. Ind. Electron. **62**, 3 (2015).
[6] W. Xu and M.-J. He, IEEE Trans. Magn. **52**, 7 (2016).
[7] Z.-H. Chen, B. Wang, Z. Chen, and Y.-G. Yan, IEEE Trans. Ind. Electron. **61**, 7 (2014).
[8] Q. Zhang, S.-R. Huang, and G.-D. Xie, IEEE Trans. Energy Convers. **25**, 4 (2010).
[9] Y.-T. Gao, D.-W. Li, R.-H. Qu, X.-G. Fan, J. Li, and H. Ding, IEEE Trans. Vehicular Tech. **67**, 1 (2018).
[10] L. Xu, W.-X. Zhao, J.-H. Ji, G.-H. Liu, Y. Du, Z.-Y. Fang, and L.-H. Mo, IEEE Trans. Magn. **50** 11 (2014).
[11] T. Kosaka, M. Sridharbabu, M. Yamamoto, and N. Matsui, IEEE Trans. Ind. Electron. **57**, 11 (2010).
[12] J. Wu and J. Yin, Chinese J. Elec. Eng. **4**, 1 (2018).